npj | clean water

Article

Published in partnership with King Fahd University of Petroleum & Minerals

https://doi.org/10.1038/s41545-024-00326-5

Fouling-resistant reverse osmosis membranes grafted with 2-aminoethanethiol having a low interaction energy with charged foulants

Jun Xiao[1,3], Shuang Hao[1,3], Yiwen Qin[1], Pengfei Qi[1], Zhaoqian Zhang[1] & Yunxia Hu[1,2]

Many fouling-resistant materials have been grafted or coated on the RO membrane surface for fouling-resistance. However, these modified RO membranes still exhibit a fast flux drop towards small charged organic foulants. Herein, we creatively use the quantum chemistry method to screen the thiol group having a close to zero interaction energy with small charged organic foulants. Thus, we selected a small molecule of 2-aminoethanethiol (AET) having a fouling-resistant thiol group and a reactive amine group for RO membrane surface modification. The water permeance of the AET-grafted RO membrane increases from 2.6 ± 0.1 L m^{-2} h^{-1} bar^{-1} to 3.2 ± 0.05 L m^{-2} h^{-1} bar^{-1}, 23% higher than that of the pristine membrane. Moreover, the AET-grafted RO membrane exhibits excellent fouling resistance against charged surfactants. Our study offers insights on the design of fouling-resistant molecules for antifouling surface modification of RO membranes towards small charged organic foulants.

Along with global population growth and industrial development, freshwater scarcity has become one of the most urgent problems that need to be addressed[1–3]. Of water treatment applications, reverse osmosis (RO) has been extensively used for water purification owing to its high separation efficiency, low energy consumption, and environmental friendliness[4–6]. Thin film composite (TFC) polyamide (PA) membranes, composed of a porous support layer and a dense active layer produced through interfacial polymerization (IP), are commonly used in the RO process[7]. However, the extensive application of RO membrane is significantly constrained by the high operation cost due to membrane fouling[8–10]. Among the major membrane fouling such as particle fouling, biofouling, scaling, and organic fouling, organic fouling particularly induced by small charged organic molecules poses the most severe challenge to RO membranes. Based on the work previously reported[8,11,12], organic molecules with a molecular weight lower than 600.0 Da are recognized as small molecular weight foulants for RO membrane fouling. These foulants originate from coking wastewater including phenolic compounds, polycyclic aromatic compounds, and heterocyclic compounds[13]. Among them, positively charged organic foulants with a low molecular weight such as DTAB (308.3 Da) and DTAC (263.9 Da), exhibit strong electrostatic attraction with the negatively charged surfaces of RO membranes having numerous carboxyl groups and thus lead to a substantial decline in water flux and significant rise in operation cost[8,14–16]. Therefore, the development of antifouling RO membranes is of utmost importance in mitigating organic fouling during the water purification process, enabling cost-effective water treatment.

It was reported that the hydrophilic surface modification of RO membranes is recognized as an effective approach to mitigate membrane fouling caused by organic foulants[17–19]. Compared with other membrane surface modification strategies such as amide activation[20], atom transfer radical polymerization (ATPR)[21,22] and others, the layer-by-layer interfacial polymerization (LbL-IP) method is a time-saving and facile method to graft fouling-resistant materials onto the polyamide surface[23–25]. Most of fouling-resistant materials are generally hydrophilic polymers such as polyvinyl alcohol (PVA)[26], polyvinylamine (PVAm)[27], polyethylene glycol (PEG)[28], zwitterionic polymers including 3-(3,4-dihydroxyphenyl)-alanine (L-DOPA)[29] and dialdehyde carboxymethyl cellulose (DACMC)[30], and

[1]State Key Laboratory of Separation Membranes and Membrane Processes, National Center for International Research on Membrane Science and Technology, School of Materials Science and Engineering, Tiangong University, Tianjin 300387, PR China. [2]Hebei Industrial Technology Research Institute of Membranes, Cangzhou Institute of Tiangong University, Cangzhou 061000, PR China. [3]These authors contributed equally: Jun Xiao, Shuang Hao.
e-mail: yunxiahu@tiangong.edu.cn

hyperbranched polymers including hyperbranched polyglycerol (hPG)[31,32], and polyethylenimine (PEI)[33,34]. Results indicate that grafting hydrophilic polymers onto the membrane surface aids in the formation of a hydration layer, which acts as a barrier to screen the hydrophobic interaction between the surface of RO membrane and foulants, thereby mitigating the extent of membrane fouling and suppressing flux decline[32]. Unfortunately, small organic foulants with positive charges and high water solubility such as dodecyl trimethyl ammonium bromide (DTAB) and dodecyl trimethyl ammonium chloride (DTAC) may penetrate into the polyamide layer and plug the pores of the RO membrane, thus leading to a substantial flux decrease and severe membrane fouling[16]. For instance, the RO membranes most commonly reported as being modified with hydrophilic materials still suffer from a severe membrane fouling with a high flux decline ratio (FDR) of approximately 40% when fouled with 50 ppm of small positively charged foulants such as DTAB or DTAC, and may even lose more than 60% flux when the foulant concentration was 100 ppm or 200 ppm[23,26,30,35]. To address these issues, significant endeavors have been made to tailor the polyamide surface charge by introducing positively charged molecules, which can enhance the membrane fouling resistance[33,36,37]. These modified RO membranes show markedly enhanced antifouling characteristics against DTAB, with an FDR of 31%, a noteworthy reduction compared to the FDR (71%) of the unmodified RO membrane and the FDR (50%) of the RO membranes by hydrophilic modification[23,38]. Nevertheless, the RO membrane modified with the positively charged materials suffers from heightened fouling from anionic small organic foulants like sodium dodecyl sulfate (SDS). This is a result of the electrostatic attraction between anionic heads of small organic foulants and cationic groups incorporated on the polyamide surface[38].

To mitigate RO membrane fouling against cationic and anionic small organic foulants simultaneously, the ideal fouling-resistant materials employe for polyamide surface grafting are highly desired to have a weak interaction energy with these typical foulants, since membrane fouling is significantly induced by the strong interaction energy between the foulants and polyamide surface[18,24]. In this work, we creatively use the quantum chemistry method to select the fouling-resistant chemical groups having a low interaction energy with both cationic and anionic small organic foulants, and then design the ideal fouling-resistant molecules based on the selected groups for RO membrane surface modification. Results reveal that the thiol group has a close to zero interaction energy with the positively charged small molecule DTAB (−0.065 eV) and the negatively charged small molecule SDS (−0.203 eV), and is expected to be an ideal chemical block of fouling-resistant materials for RO membrane surface modification. Meanwhile, we notice that 2-aminoethanethiol (AET) is a small molecule containing a reactive amino group and a hydrophilic thiol group, which makes it a promising material for polyamide surface modification since amino groups are reactive with acyl chloride and thiol groups are fouling resistant towards small charged molecules.

Herein, AET was grafted onto the surface of the RO membrane by the LbL-IP process to improve the membrane fouling resistance against small organic foulants, particularly small-molecular-weight charged surfactants, as illustrated in Fig. 1. We systematically investigated the effects of different AET concentrations (0.02 wt.%, 0.04 wt.%, 0.06 wt.) on the surface properties, separation performance, and antifouling performance of the RO membranes. Furthermore, we also developed a post-treatment approach to enhance the stability of the AET-grafted RO membrane. The antifouling properties of the AET-grafted RO membrane against differently charged small foulants were assessed by a RO system, while the antifouling mechanisms of RO membranes were also explored using quartz crystal microbalance with dissipation (QCM-D). The importance of our research lies in the selecting of AET molecules for antifouling surface modification of RO membranes. This is attributed to the reactivity of its amino groups with the RO membrane and the close to zero interaction energy of its thiol groups with DTAB (−0.065 eV) and SDS (−0.203 eV). Our study offers insights on the design of fouling-resistant molecules for antifouling surface modification of RO membranes towards both positively and negatively charged small organic foulants.

Results and discussion

Characterization of RO membranes before and after AET modification

The RO membrane was modified with different AET concentrations (0.02 wt%, 0.04 wt%, and 0.06 wt%) *via* a LbL-IP method (Fig. 1). In order to verify the successful AET grafting, the surface elemental compositions of the PAs were detected by XPS as shown in Table 1. With the increasing AET concentration, the atomic percentage of S on the modified membrane surface increases from 0% to 1.17%, 1.96%, 2.78%, and the atomic ratio of S/O increases from 0 to 0.104, 0.165, and 0.243, respectively. The results indicate that more AET molecules were introduced onto the membrane surface with higher AET concentrations. And the corresponding grafting ratio (GR) of AET was calculated as 17.9%, 19.2%, and 20.8% with the increasing AET concentration from 0.02 wt%, 0.04 wt% to 0.06 wt% (as shown in Supplementary Note 1 and Supplementary Fig. 1). However, no absorption peak of thiol groups appears in the ATR-IR spectrum after AET grafting because a limited amount of the AET molecules grafted on the membrane surface is undetected by IR (Supplementary Fig. 2). Figure 2 presents that both surfaces of the pristine membrane and the AET-grafted membrane exhibit a representative leaf-like structure[34,38–40] with the roughness (R_a) of 71.7 ± 7.3 nm for the pristine membrane, and 49.0 ± 4.7 nm, 46.0 ± 4.1 nm, 42.3 ± 4.2 nm for the AET-grafted membrane with the increasing AET concentration from 0.02 wt% to 0.06 wt%. The surface roughness of the AET-grafted membrane experiences an obvious decrease compared with the pristine membrane, and exhibits a comparable R_a with the increasing AET grafting concentration.

The surface properties of the RO membranes including water contact angle (WCA) and surface charge were further evaluated. As depicted in Fig. 3a, with the increasing AET grafting ratio, the WCA values of the modified membrane experience a decrease from 76.3 ± 2.8° to 50.3 ± 2.4° for the sample modified with 0.02 wt% AET, and 50.8 ± 9.8° for the sample modified with 0.04 wt% AET. However, the WCA value of the modified membrane increases to 61.0 ± 1.5° when 0.06 wt.% AET was used for RO membrane surface modification, which might be caused by the formation of

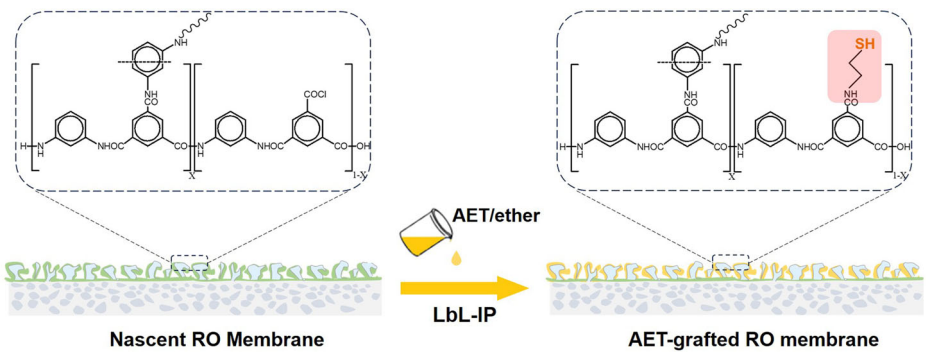

Fig. 1 | Schematic diagram of fabrication of the AET-grafted RO membranes. Experimental conditions: the top surface of the PSf UF membrane was soaked in an aqueous monomer solution of 2 wt% MPD for 2 min. Then, an organic monomer solution of 0.1 wt% TMC in n-hexane was poured onto the MPD-pregnant membrane surface for 1 min, followed by 2 min incubation with a AET solution (0.02 wt%, 0.04 wt%, 0.06 wt% AET) in ether. Subsequently, the membrane was subjected to a 10-min treatment in an air oven at 60 °C to obtain the AET-grafted RO membrane.

hydrophobic disulfide bonds (-S-S-) under the high concentration of AET (discussed in section 3.2). Furthermore, the surface zeta potential of AET-grafted membrane increased from −46.1 ± 1.1 mV to −35.0 ± 1.2 mV, −33.1 ± 3.2 mV, and −30.4 ± 2.7 mV (at pH=7) when the membrane was modified with 0.02 wt%, 0.04 wt%, and 0.06 wt% AET, respectively (Fig. 3b). This increase in zeta potential can be attributed to the reduce of the number of the carboxylic groups resulting from the hydrolysis of residual acyl chloride groups[41,42], as shown in Supplementary Fig. 3.

The separation properties and fouling resistance of the RO membranes were explored before and after the AET grafting. The water permeance increases from 2.6 ± 0.1 L m^{-2} h^{-1} bar^{-1} for the pristine membrane to 3.2 ± 0.02 L m^{-2} h^{-1} bar^{-1} and 3.2 ± 0.05 L m^{-2} h^{-1} bar^{-1} for the AET-grafted membrane with AET having the increasing concentrations from 0.02 wt% to 0.04 wt%, respectively. While, the water permeance of the modified membrane decreases to 2.9 ± 0.19 L m^{-2} h^{-1} bar^{-1} for the sample modified with 0.06 wt% AET. This decrease is mainly attributed to the increasing mass transfer resistance from the RO membrane grafted with more AET[16]. The NaCl rejection rate of the AET-grafted membrane remains constant (~ 99.0%) regardless of the AET grafting concentration. To further evaluate the anti-fouling properties of the membrane, DTAB and SDS were screened as model foulants. With the increasing AET concentration, the FDR towards DTAB of the AET-grafted membrane decreases dramatically from 70.4% (pristine membrane) to 57.6% (M-0.02), 43.7% (M-0.04), and 40.0% (M-0.06), respectively (Figs. 3d and 5). Results suggest that the antifouling properties of the RO membranes towards DTAB is improved significantly with the substantially decreased FDR by grafting AET onto the RO membrane surface. This phenomenon could be attributed to two aspects: (1) the AET-grafted RO membranes exhibit better hydrophilic properties (lower WCA) than the pristine RO membrane owing to grafting of hydrophilic -SH groups[43]; (2) the surface charge of the AET-grafted membranes is less negative because some residual acid chlorides are consumed for AET grafting. The FDR towards SDS of the AET-grafted membrane with an AET concentration of 0.02 wt % is 29.5%, comparable to the value of 27.6% for the pristine membrane. However, the AET-grafted membranes exhibit severe membrane fouling towards SDS, especially when the membrane was modified with 0.06 wt% AET. This may be ascribed to the strong electrostatic attraction between SDS and free amine groups (Supplementary Fig. 4) detected on the modified PA since AET molecules with amine groups are attached on the PA surface through disulfide bonds (-S-S-) formation. It can be concluded that the AET concentration is a critical parameter to significantly affect the amount of AET grafted onto the RO membrane surface and thus governs the surface properties, and then influences perm-selectivity and antifouling properties of the RO membranes. As discussed above, the AET-grafted RO membrane with an AET concentration of 0.04 wt% was selected for further analysis.

Table 1 | The elemental compositions of the AET-grafted RO membranes modified with AET having the increasing concentrations from 0.02 wt.% to 0.06 wt.% (M-0.02 for 0.02 wt%, M-0.04 for 0.04 wt%, M-0.06 for 0.06 wt%) measured by XPS

Membrane	C (%)	*N* (%)	O (%)	S (%)	S/O	Grafting ratio (%)
pristine membrane	75.29	11.12	13.59	0		
M-0.02	75.72	10.45	12.53	1.30	0.10	17.9
M-0.04	75.59	10.63	11.82	1.96	0.16	19.2
M-0.06	76.04	9.73	11.44	2.78	0.24	20.8

Post-treatment of the AET-grafted RO membrane

To break the formation of the disulfide bonds (-S-S-) on the AET-grafted RO membrane surface and to prevent un-grafted AET molecules from attaching on the membrane surface, thus alleviating the SDS absorption on the AET-grafted membrane. The AET-grafted RO membrane modified with an AET concentration of 0.04 wt% was treated with 10 mmol/L TCEP in 10 mmol/L tris-buffer (pH = 7.5) for 30 min[44,45]. As shown in Table 2 and Supplementary Fig. 5, the peak area ratio of disulfide bonds (-S-S-) to sulfhydryl groups (-SH) on the surface of the post-treated membrane decreases significantly from 0.32 to 0.12. This indicates that the TCEP post-treatment can effectively reduce disulfide bonds to sulfhydryl groups on the membrane surface. TCEP post-treatment did not change the membrane morphologies or separation properties of the pristine membrane, as shown in Supplementary Fig. 6.

In addition, the surface hydrophobicity and charge properties were characterized to further investigate the influence of the TCEP post-treatment. As Fig. 4a, b shows, the membrane surface zeta potential (at pH = 7) slightly decreases from −33.1 ± 3.2 mV to −37.1 ± 3.0 mV after the post-treatment, and the WCA of the post-treated membrane experiences a decrease from 50.8 ± 9.8° to 35.4 ± 0.6°. These changes can be attributed to the conversion of hydrophobic disulfide bonds to hydrophilic thiol groups on the membrane surface. Furthermore, the membrane water permeance does not change much (Fig. 4c) after the post-treatment. However, the membrane salt rejection decreases from 99.0 ± 0.03% to 98.5 ± 0.04%. This may be because the removal of AET attached on the membrane surface through the disulfide bonds (-S-S-) makes the PA loose with low salt transport resistance. In addition, the long-term operational stability of the AET-grafted and post-treated RO membranes was valued by a 72-h cross-flow test at 15 bar in a RO system. As Supplementary Fig. 7 shows, the water permeance of both the AET-grafted and the post-treated RO membranes decreases slightly over time, while the salt rejection increases during the test, which is a typical compaction effect under a high operating pressure. Overall, results suggest that both the AET-grafted and post-treated RO membranes possess good long-term operational stability. In addition, the stability of the post-treated membrane after long-term storage was also evaluated. The membrane underwent a pore-preservation treatment and was stored in a room environment. After 15 and 30 days of storage, the post-treated

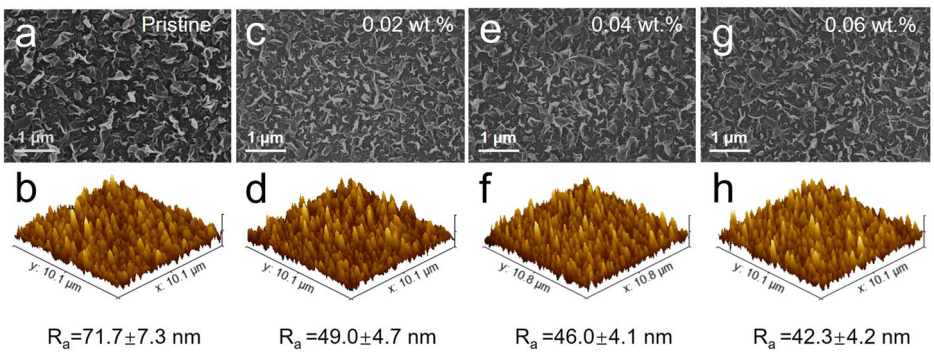

Fig. 2 | Surface morphology characterization of RO membranes before and after AET modification. SEM (top) and AFM (bottom) images of the pristine RO membrane **a**, **b** and the AET-grafted RO membranes **c**, **d** modified with 0.02 wt% AET; **e**, **f** modified with 0.04 wt% AET; **g**, **h** modified with 0.06 wt% AET. Error bars represent the standard deviations from three separate experiments.

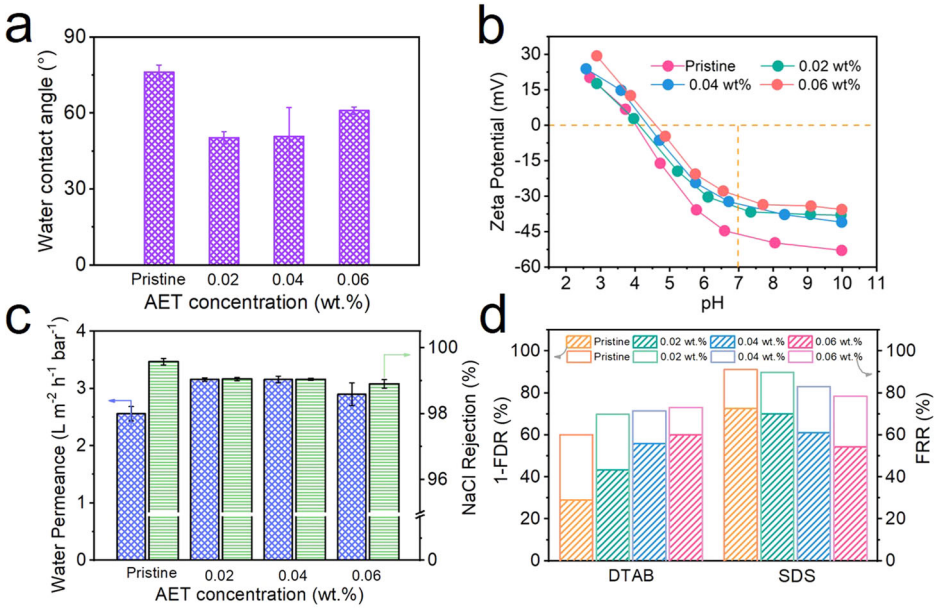

Fig. 3 | Surface properties, separation performance and antifouling properties of RO membranes before and after AET modification. Water contact angle **a**, zeta potential **b**, separation performance **c**, and antifouling performance **d** of the pristine RO membrane RO membrane and the AET-grafted RO membranes modified with different AET concentrations (0.02 wt%, 0.04 wt%, 0.06 wt%). Error bars represent the standard deviations from three separate experiments.

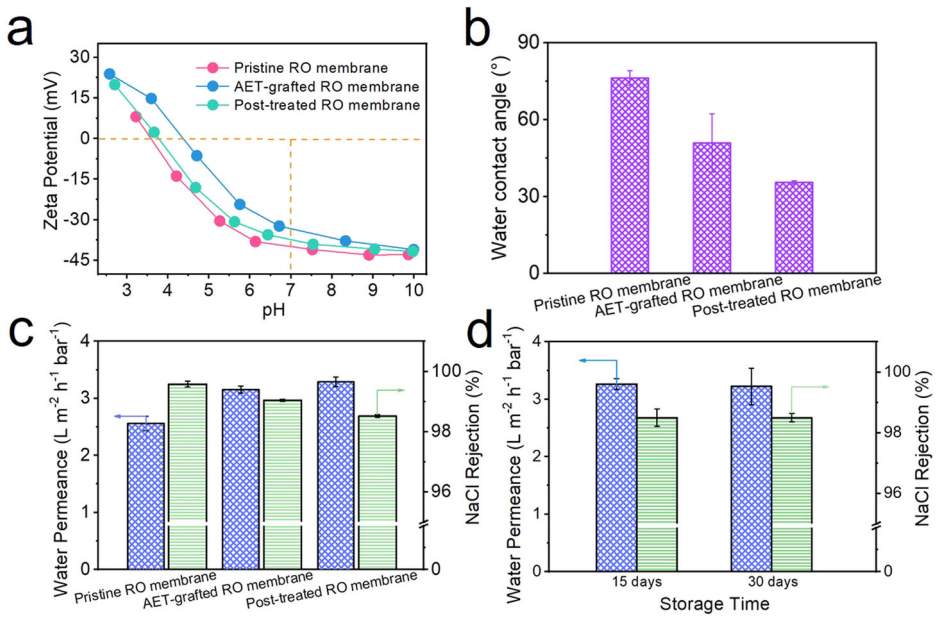

Fig. 4 | Surface properties and separation performance of RO membranes before and after post-treatment and long-term storage. Zeta potential **a**, water contact angle **b**, separation performance **c** of the pristine RO membrane, the AET-grafted RO membrane (AET concentration: 0.04 wt%), and the post-treated RO membrane, and separation performance **d** of the post-treated membrane with storage time. Error bars represent the standard deviations from three separate experiments.

membrane retains a stable separation performance, with the water permeance above 3.3 ± 0.08 L m^{-2} h^{-1} bar^{-1} and the NaCl rejection above 98.5% (Fig. 4d). These results suggest that the post-treated membrane can maintain its separation performance even after long-term storage, making it suitable for practical applications.

Table 2 | The elemental compositions of the pristine, the AET-grafted (0.04 wt% AET), and the post-treated RO membranes measured by XPS (the area percentage of S 2p peaks detected at 163.4–164.3 eV (-SH), 164.8–165.3 eV (-S-S-) are calculated)

Membrane	C (%)	*N* (%)	O (%)	S (%)	S/O	-S-S-/-SH
Pristine RO	75.29	11.12	13.59	—	—	—
AET-grafted RO	75.59	10.63	11.82	1.96	0.16	0.32
Post-treated RO	75.44	10.69	11.94	1.93	0.16	0.12

Antifouling performance and mechanism of the post-treated RO membrane

The fouling resistance of the post-treated RO membrane was further studied against model foulants of differently charged surfactants (SDS and DTAB) and proteins (LYZ and BSA). As illustrated in Fig. 5, for the negatively charged surfactant SDS, the post-treated membrane exhibits significantly better antifouling performance with a lower FDR of 31.3% compared to the AET-grafted membrane with an FDR of 38.4%. This can be attributed to more negatively charged and hydrophilic membrane surface obtained from the reduction of the disulfide bonds (-S-S-) into sulfhydryl groups (-SH) during the post-treatment. The FRR towards SDS of the post-treated membrane is 87.3%, which is lower than that of the AET-grafted membrane with an FRR of 82.2%. This may be because of the stronger electrostatic repulsion between negatively charged surfactant SDS and the negatively charged surface of the post-treated membrane compared with the AET-grafted membrane, making it less prone to SDS adsorption under shear

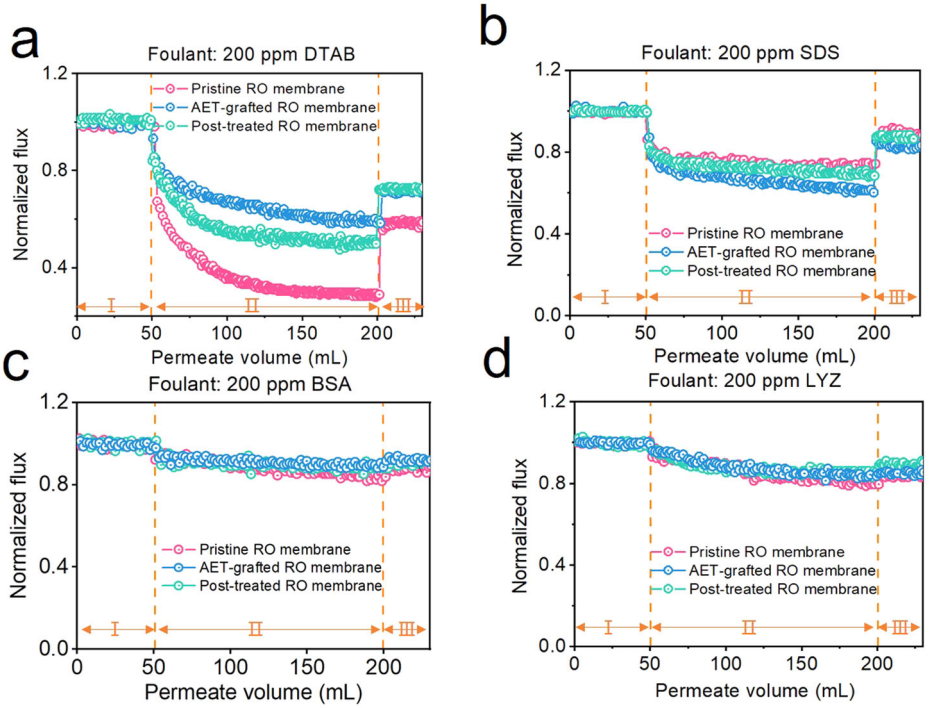

Fig. 5 | Antifouling performance of RO membranes. Flux profiles of the pristine RO membrane, the AET-grafted RO membrane (AET concentration: 0.04 wt%), and the post-treated RO membrane during the fouling and cleaning processes in a cross-flow RO test. The RO test contains three processes including the first stabilization stage (I), the fouling stage (II), and the cleaning stage (III). The feed solution in each stage is as follows: (I) 2000 ppm NaCl, (II) 2000 ppm NaCl and 200 ppm foulants (DTAB for (**a**), SDS for (**b**), BSA for (**c**), or LYZ for (**d**), and (III) 2000 ppm NaCl.

force. Additionally, the FDR of the post-treated membrane when fouled with DTAB is 50.1%, which is higher than the value of 43.7% for the AET-grafted membrane, but still significantly better than the pristine membrane (70.4%). Furthermore, the FDR of the post-treated membrane towards LYZ and BSA is 14.0% and 10.4%, respectively, much higher than both the pristine and AET-grafted membranes. Both the positively charged protein LYZ and the negatively charged protein BSA induce a slower and less water flux decline than the charged surfactants with small molecular weights. This is because charged surfactants such as DTAB with small molecular weight may penetrate into the polyamide layer and plug the pores of RO membrane surface, thus leading to higher flux drop and more severe membrane fouling compared with proteins[16].

Supplementary Table 1 and Supplementary Fig. 8 summarize the most recent progress in the development of antifouling RO membranes. The calculations for 1- FDR and 1- FRR are based on the flux decline profiles. Membrane surface modification through coating or grafting fouling-resistant materials is the most widely reported method to improve the antifouling abilities of RO membranes. Surface coating benefits from weakened interactions between membrane surface and foulants, reducing the deposition of foulants onto polyamide surface. However, most of coatings such as polyvinyl alcohol (PVA), polydopamine (PDA), and polyethylene glycol (PEG), have limitations during long-term operation due to instability, which is attributed to physical interactions like hydrogen bonding, electrostatic interaction, or van der Walls. Moreover, the water permeance of RO membrane may be decreased because of high water transport resistance from the extra coating layer. Compared with surface coating, molecules could directly graft onto membrane surface *via* chemical bonds without increasing transport resistance by surface grafting. The RO membranes modified with hydrophilic materials including PVAm, hPG, DACMC, QDAP, or DEA present significantly improved antifouling performance with a low FDR of approximately 30% against SDS, while, the FDR towards DTAB reaches 60%, which is due to the limitations of grafted hydrophilic materials in effectively mitigating electrostatic effects between the membrane surface and DTAB. Hence, charged molecules are grafted onto the RO membrane to improve the antifouling performance against DTAB, the RO membranes modified with charged molecules such as AEGu, DMEDA, PL, or PEI show a decreased negative surface charge with a zeta potential of −20 mV ~ −10 mV (pH = 7), and thus exhibiting a low FDR of only 40% towards DTAB. While, these modified RO membranes suffer from a high FDR of approximately 50% against SDS, which can be attributed to the electrostatic attraction between the grafting molecules with opposite charges and the foulants. In contrast, the AET modified RO membrane in this work exhibits excellent fouling resistance against both DTAB and SDS with FDRs of 43.5% and 31.3%, respectively. This is because of the low interaction energy of AET molecules with charged organic foulants. Overall, the AET-grafted RO membrane with excellent fouling resistance and good separation performance in this study shows a great promise for practical applications.

To investigate the deposition behavior of foulants on the RO membrane surface, we employed QCM-D to measure the absorption and desorption of SDS and DTAB (200 ppm) on the membrane surface. The Kevin-Voigt model was utilized to calculate the adsorbed mass of the fouling layer. Figure 6a illustrates that upon exposure to DTAB, all PA samples experience a rapid adsorption phase with a quick mass increase, followed by a significant decrease in the adsorption rate. The gained mass of the pristine PA, the AET-grafted and post-treated PAs are 1214 ± 78 ng/cm^2, 576 ± 38 ng/cm^2, and 752 ± 60 ng/cm^2, respectively. Furthermore, the deposited foulants on the membrane surface were characterized by dissipation (ΔD) and frequency (Δf) values, and a higher $|\Delta D/\Delta f|$ value indicates a looser foulant layer on the membrane surface[16,31], as shown in Supplementary Table 2. Moreover, the *D-f* plot is shown in Fig. 6c, d, all membranes saw rapid dissipation shift decline, followed by the gradually suppressed dissipation shift decline when the membrane fouled with DTAB or SDS. By comparing the slopes of the curves, the AET-grafted membrane and the post-treated membrane exhibit higher absolute value of slope than the pristine RO membrane towards both DTAB and SDS during the QCM-D measurements. These results indicate the foulant layer deposited on the PA surfaces of both the AET-grafted and post-treated RO membranes is softer and looser, resulting in a reduced adhesion between the foulants and the surface of RO membrane compared to the pristine PA. After 1 h of DI water cleaning, the mass desorption/adsorption ratios for the pristine, AET-grafted, and post-treated RO membranes are 20.3 ± 1.2%, 27.8 ± 0.7%, and 35.5 ± 1.3%, respectively, corresponding to the FRR trend described above: post-treated RO membrane > AET-grafted RO membrane > pristine RO membrane. In the case of SDS, the total mass of SDS adsorbed on the

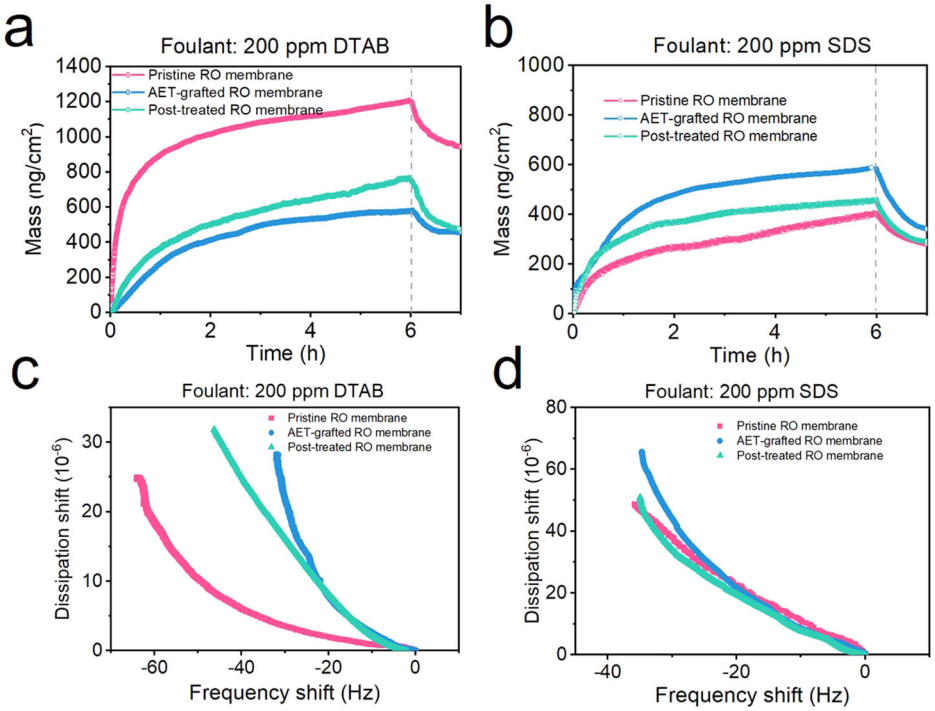

Fig. 6 | Absorption properties of foulants on the PA surface characterized by QCM-D. Absorption and desorption behaviors of DTAB **a** and SDS **b** on the PA surfaces prepared from the pristine, the AET-grafted (AET concentration: 0.04 wt%), and post-treated RO membranes, properties of absorbed DTAB **c**, and SDS **d** layers on the RO membranes were monitored by QCM-D.

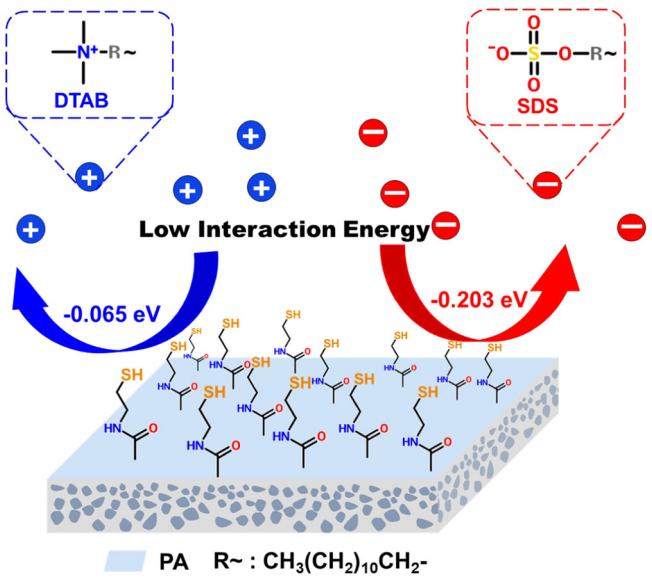

Fig. 7 | The proposed antifouling mechanism of the RO membranes. The interaction energy between sulfhydryl groups (-SH) and surfactants is −0.065 eV and −0.203 eV, for cationic DTAB and anionic SDS, respectively.

pristine, AET-grafted, and post-treated PAs are 411 ± 29 ng/cm^2, 578 ± 54 ng/cm^2, and 460 ± 31 ng/cm^2, respectively, much lower than the total mass of DTAB absorbed on the PA surface, because the PA exhibits strong electrostatic repulsion with SDS, while, strong electrostatic attraction with DTAB. The mass desorption/adsorption ratios for the corresponding membranes are 37.1 ± 0.9%, 43.7 ± 2.7%, and 39.6 ± 1.1%, indicating that the SDS foulant layer could be easier to be removed from the AET-grafted and post-treated PAs than that from the pristine PA. In summary, our results demonstrate that the AET-grafted and post-treated RO membranes significantly improve the antifouling performance towards DTAB in contrast to the pristine membrane, and the post-treated membrane exhibits comparable antifouling performance towards SDS with the pristine membrane.

In this work, we use the quantum chemistry calculation to screen out the antifouling groups towards small charged foulants, cationic DTAB and anionic SDS were selected as model foulants. The results indicate that thiol group (-SH) having a low interaction energy with DTAB (−0.065 eV) and anionic SDS (−0.203 eV), respectively, as shown in Fig. 7. 2-aminoethanethiol (AET) is a small molecule containing a reactive amino group and a hydrophilic thiol group, and thus AET was grafted onto the surface of the RO membrane via the LbL-IP process. The RO membranes grafted with AET exhibit excellent fouling resistance with absorption mass of 576 ± 38 ng/cm^2 and 578 ± 54 ng/cm^2. Furthermore, the grafting of small AET molecules could be beneficial to the improvement of surface coverage of fouling-resistant molecules on the RO membrane surface, which effectively regulates the surface properties (more hydrophilic and less electronegative) and thus enhances the membrane antifouling performance. Therefore, the surface grafting of AET on the membrane can effectively improve the fouling resistance of the RO membrane. Our study offers insights on the design of fouling-resistant molecules for antifouling surface modification of RO membranes towards small charged foulants.

Methods

Materials

M-phenylenediamine (MPD, 99%), tris (hydroxymethyl) methyl aminomethane (Tris, 99%), trimesoyl chloride (TMC, 99%) and 2-aminoethanethiol (AET, 97%) were obtained from J&K Scientific Co. Ltd. (Beijing, China). Sodium dodecyl sulfonate (SDS, 99%), polyvinyl alcohol (PVA, 99%), bovine serum albumin (BSA, 96%), dodecyl trimethyl ammonium bromide (DTAB, 99%), (±)-10-camphor sulfonic acid (CSA, 99%) and tris (2-carboxyethyl) phosphine (TCEP, 98%) were obtained from Aladdin Co. Ltd. (Shanghai, China). Polysulfone ultrafiltration membrane (PSf UF, MWCO: 30 kDa) was supplied by Beichuang qingyuan Co. Ltd. (Beijing, China). Lysozyme (LYZ, 99%) was purchased by Macklin Co. Ltd. (Shanghai, China). Anhydrous diethyl ether (99%) was ordered from Fengchuan reagent technology Co. Ltd. (Tianjin, China). Other chemicals

were purchased from Tianjin Kemiou Chemical Reagent Co. Ltd. (Tianjin, China), including triethylamine (TEA, 99%), *n*-Hexane, sodium hydrogen sulfite ($NaHSO_3$, 99.7%), glycerol (99%), isopropyl alcohol (IPA, 99%), sodium chloride (NaCl, 99%), dimethylacetamide (DMAC, 99%).

Preparation of RO membranes

Preparation of AET-grafted RO membranes: The AET-grafted RO membranes were fabricated *via* the LbL-IP method with the PSf UF membranes as supports, as shown in Fig. 1. MPD (2 wt%), CSA (2.4 wt%) and TEA (1.1 wt%) were dissolved in deionized (DI) water to prepare an aqueous solution of MPD monomer. TMC in n-hexane solution (0.1 wt%) served as the organic monomer solution. The top surface of the PSf UF membrane was immersed in 15 mL aqueous solution of MPD monomer for 2 min, and then immersed in 15 mL organic solution of TMC monomer for 1 min to prepare a nascent polyamide layer. After that, the membrane surface was exposed to 15 mL AET solution (different concentrations of AET with 0.02 wt%, 0.04 wt%, and 0.06 wt%) in diethyl ether for 2 min to modify the RO membrane by the reaction between the reaction residual acyl chloride groups of nascent polyamide and the amino group of AET molecules. Subsequently, the membrane was subjected to a 10-min treatment in an air oven at 60 °C. The pristine RO membrane, serving as the control membrane, was obtained without AET modification. The RO membrane modified with AET molecules was termed as the AET-grafted RO membrane.

Post-treatment and preservation: The AET-grafted RO membrane (made from 0.04 wt% AET) was soaked in 20 ml TCEP solution (10 mmol/L) for 30 min, followed by a brief DI water rinsing, and the obtained membrane was named as the post-treated RO membrane. Then, the post-treated RO membrane was soaked in a preservative (6 wt% glycerol, 0.1 wt% SDS, 1 wt% IPA, and 1 wt% PVA in DI water) for 2 min and subsequently put into the air-dry oven at 70 °C for 3 min and then stored in a room environment.

Membrane characterization

The surface morphology of the RO membrane was imaged by Germini SEM500 scanning electron microscopy with an accelerating voltage of 10 kV (SEM, Zeiss, Japan). Membrane samples were attached to the sample holder by a conductive adhesive after being coated with platinum (Pt). The surface roughness was observed by atomic force microscopy (AFM, Bruker Optics, Germany). The samples were imaged at a tapping mode and then analyzed using the Gwyddion software. R_a refers to the arithmetic average roughness and is calculated from the average of the height deviations from the mean height at each point on the membrane surface. The membrane surface composition was analyzed by x-ray photoelectron spectroscopy (XPS, Thermo Fisher, Kα, USA). The data were recorded by setting the take-off angle of the X-rays at 60°. The chemical groups of the membrane were characterized by an ATR-FTIR spectrometer (Thermo Scientific, Nicolet iS10, USA). The surface hydrophobicity was detected by a contact angle analyzer (Kruss, Germany). A water droplet of 2 μL was dropped on the naturally dried membrane surfaces and imaged after 8 s. The data were analyzed using the Advance software. To reduce the experimental errors, the contact angle was measured at least at five random locations of the membrane and the average values were reported. The streaming surface zeta potential was measured by SurPASS 3 Zeta potential analyzer (Anton Paar GmbH, Austria) at a pH range from 3 to 10, using KCl (1 mM) as an electrolyte.

Desalination properties and dynamic fouling measurements in the RO process

Desalination properties measurements: A customized cross-flow system that has an effective filtration area of 28.26 cm^2 was employed to evaluate the filtration performance of the RO membrane. To ensure a stable membrane flux, the membranes were pre-pressurized at 20 bar for 1 h. Subsequently, the desalination properties of RO membranes were assessed using a feed solution (2000 ppm NaCl) at 15 bar and 25 ± 0.2 °C. The membrane water permeance (A) and salt rejection (R) were obtained through Eq. (1) and Eq. (2), respectively.

$$A = \frac{\Delta V}{S \times \Delta t \times P} \tag{1}$$

$$R = \left(1 - \frac{C_p}{C_f}\right) \times 100\% \tag{2}$$

Where ΔV is permeation volume (L), S is effective filtration area (28.26 cm^2), Δt is evaluation time (h), P is evaluation pressure (bar). C_f and C_p are solute concentrations of feed and permeate solution.

Dynamic fouling measurements: Dynamic fouling measurements were conducted employing the above-mentioned cross-flow RO set up with SDS, LYZ, DTAB and BSA as model foulants. Firstly, the initial permeate flux (J_0) of the RO membrane was assessed at 15 bar for 30 min using a NaCl feed solution (2000 ppm) with a cross-flow rate of 1.5 L/min after pre-pressurizing the membrane for one hour at 20 bar. Subsequently, the feed solution was supplemented with an organic model foulant of SDS or DTAB to achieve a specified concentration (200 ppm), and the permeate flux (J_t) was measured during the fouling process for 4 h. Finally, the RO membrane was cleaned upon 10 min DI water flushing for 3 times with a cross-flow rate of 3 L/min at 5 bar, and then the recovered permeate flux (J_{wc}) was evaluated using a NaCl feed solution (2000 ppm) at 15 bar for 30 min. The flux decline ratio (FDR) and flux recovery ratio (FRR) are determined by Eq. (3) and Eq. (4), respectively.

$$FDR = \left(1 - \frac{J_t}{J_0}\right) \times 100\% \tag{3}$$

$$FRR = \frac{J_{wc}}{J_0} \times 100\% \tag{4}$$

Membrane surface fouling mechanism evaluation by *QCM-D*

The absorption of foulants on the polyamide surface was evaluated by QCM-D (E4 system, Q-sense, Sweden), following our earlier reported work[16]. Briefly, the RO membrane was immersed in DMAC to dissolve the PSf UF supporting layer and to obtain the free-standing PA active layer, which was subsequently transferred onto the quartz crystal gold sensor and then dried at 40 °C all night. The gold sensor, with the free-standing PA active layer coated, was placed into the chamber and stabilized with air initially. Then, DI water was introduced to the active layer surface with a flow rate of 50 μL/min for a period of time till both dissipation (D) and frequency (f) of the sensor stabilized. Odd overtones including 3th, 5th, 7th, 9th, 11th and 13th of the sensor were selected due to the information collected from even overtones overlapping to some extent. The adsorption and desorption characteristics of the foulants on the PA surface were monitored during the fouling and cleaning processes. During the fouling process, a foulant solution of 200 ppm DTAB or 200 ppm SDS was introduced to the active layer surface, and the mass variation of the polyamide was monitored for a period of time (6 h). Lastly, the deionized water was introduced to clean the polyamide surface for removing the loosely absorbed foulants for 0.5 h, the mass variation of the recovered polyamide was monitored for a period of time (6 h). After the QCM-D measurement, the gold sensor was immersed in a mixture (a 5:1:1 mixture of DI water, highly corrosive ammonia (25%), and strongly oxidizing hydrogen peroxide (30%)) to completely desorb the polyamide layer at 75 °C for 30 min. Subsequently, the sensor was rinsed with DI water to remove the residual mixture. Finally, the senser was dried with nitrogen gas and stored for further use.

Quantum chemistry calculation

Quantum chemistry is used to simulate the molecular behavior via quantum mechanics. Upon consulting the literature[16,46], the density function theory (DFT) calculation was conducted to obtain the optimal adsorption

configurations and calculate the molecule-to-molecule interaction energy. In our work, a series of chemical groups, such as the sulfhydryl group (-SH), hydroxyl group (-OH), carboxyl group (-COOH), amino group (NH_2), and amide bond (-CONH), were assessed. Positively charged small molecule DTAB and negatively charged small molecule SDS were selected as the model foulants. Prior to calculation, the distance between DTAB or SDS and the chemical group was meticulously set to 1 nm using B3LYP by Gauss-View 5.0. Subsequently, the interaction energy between the model foulant and the respective chemical group was rigorously assessed by DFT, as shown in Eq. (5). As shown in Supplementary Table 3, the results reveal that a sulfhydryl group has a close to zero interaction energy with DTAB (−0.065 eV) and SDS (−0.203 eV), and is expected to be an ideal chemical block of fouling-resistant materials for RO membrane surface modification.

$$E_q = E_{total} - E_A - E_B \quad (5)$$

Where E_q is interaction energy, E_A is the energy of the model foulant, E_B is the energy of the chemical group, E_{total} represents the total energy of the system.

Data availability

The data that support the findings of this study are available from the corresponding author upon reasonable request.

Code availability

For access to detailed code information, please contact the corresponding author directly.

Received: 4 September 2023; Accepted: 5 April 2024;
Published online: 18 April 2024

References

1. Elimelech, M. & Phillip, W. A. The future of seawater desalination: energy, technology, and the environment. *Science* **333**, 712–717 (2011).
2. Lu, X. & Elimelech, M. Fabrication of desalination membranes by interfacial polymerization: history, current efforts, and future directions. *Chem. Soc. Rev.* **50**, 6290–6307 (2021).
3. Ly, Q. V. et al. Characteristics and influencing factors of organic fouling in forward osmosis operation for wastewater applications: a comprehensive review. *Environ. Int.* **129**, 164–184 (2019).
4. Shannon, M. A. et al. Science and technology for water purification in the coming decades. *Nature.* **452**, 301–310 (2008).
5. Tawalbeh, M. et al. Insights on the development of enhanced antifouling reverse osmosis membranes: Industrial applications and challenges. *Desalination* **553**, 116460 (2023).
6. Hu, Y. Grand challenge in membrane applications: Liquid. *Front. Membr. Sci. Technol.* **2**, 1177528 (2023).
7. Freger, V. & Ramon, G. Z. Polyamide desalination membranes: Formation, structure, and properties. *Prog. Polym. Sci.* **122**, 101451 (2021).
8. Zhang, R. et al. Antifouling membranes for sustainable water purification: strategies and mechanisms. *Chem. Soc. Rev.* **45**, 5888–5924 (2016).
9. Singh, S. K. et al. Fouling limitations of osmotic pressure-driven processes and its remedial strategies: a review. *J. Appl. Polym. Sci.* **140**, e53295 (2023).
10. Choudhury, R. R. et al. Antifouling, fouling release and antimicrobial materials for surface modification of reverse osmosis and nanofiltration membranes. *J. Mater. Chem. A.* **6**, 313–333 (2018).
11. Jian, C. et al. Low molecular weight hydrogel for super efficient separation of small organic molecules based on size effect. *ACS Sustain. Chem. Eng.* **7**, 11062–11068 (2019).
12. Shon, H. K., Vigneswaran, S. & Cho, J. Comparison of physico-chemical pretreatment methods to seawater reverse osmosis: detailed analyses of molecular weight distribution of organic matter in initial stage. *J. Membr. Sci.* **320**, 151–158 (2008).
13. Tamang, M. & Paul, K. K. Advances in treatment of coking wastewater–a state of art review. *Water Sci. Technol.* **85**, 449–473 (2022).
14. She, Q. et al. Membrane fouling in osmotically driven membrane processes: a review. *J. Membr. Sci.* **499**, 201–233 (2016).
15. Liu, C. et al. Separation, anti-fouling, and chlorine resistance of the polyamide reverse osmosis membrane: from mechanisms to mitigation strategies. *Water Res.* **195**, 116976 (2021).
16. Zhang, S. et al. Optimization and organic fouling behavior of zwitterion-modified thin-film composite polyamide membrane for water reclamation: a comprehensive study. *J. Membr. Sci.* **596**, 117748 (2020).
17. Asadollahi, M. et al. Enhancement of surface properties and performance of reverse osmosis membranes after surface modification: a review. *Desalination* **420**, 330–383 (2017).
18. Hu, Q. et al. The effect of surficial function groups on the anti-fouling and anti-scaling performance of thin-film composite reverse osmosis membranes. *J. Membr. Sci.* **668**, 121276 (2023).
19. Zhao, X. et al. Antifouling membrane surface construction: chemistry plays a critical role. *J. Membr. Sci.* **551**, 145–171 (2018).
20. Li, X. et al. Surface modification of polyamide nanofiltration membrane by grafting zwitterionic polymers to improve the antifouling property. *J. Appl. Polym. Sci.* **131**, 41144 (2014).
21. Ginic-Markovic, M. et al. Biofouling resistance of polysulfobetaine coated reverse osmosis membranes. *Desalination* **369**, 37–45 (2015).
22. Goh, P. S. et al. Contemporary antibiofouling modifications of reverse osmosis desalination membrane: a review. *Desalination* **468**, 114072 (2019).
23. Wang, J. et al. In situ surface modification of thin-film composite polyamide membrane with zwitterions for enhanced chlorine resistance and transport properties. *ACS Appl. Mater. Interfaces.* **11**, 12043–12052 (2019).
24. Zhao, Q. et al. Construction of tunable "silica molecular brush" on the polyamide membrane surface for enhancing water permeability and antifouling performance. *Desalination* **554**, 116521 (2023).
25. Gu, J. E. et al. Molecular layer-by-layer assembled thin-film composite membranes for water desalination. *Adv. Mater.* **25**, 4778–4782 (2013).
26. Liu, M. et al. Improving fouling resistance and chlorine stability of aromatic polyamide thin-film composite RO membrane by surface grafting of polyvinyl alcohol (PVA). *Desalination* **367**, 11–20 (2015).
27. Wu, J. et al. Polyvinylamine-grafted polyamide reverse osmosis membrane with improved antifouling property. *J. Membr. Sci.* **495**, 1–13 (2015).
28. Ray, J. R. et al. Antiscaling efficacy of $CaCO_3$ and $CaSO_4$ on polyethylene glycol (PEG)-modified reverse osmosis membranes in the presence of humic acid: interplay of membrane surface properties and water chemistry. *Chem. Chem. Phys.* **19**, 5647–5657 (2017).
29. Azari, S. & Zou, L. Using zwitterionic amino acid l-DOPA to modify the surface of thin film composite polyamide reverse osmosis membranes to increase their fouling resistance. *J. Membr. Sci.* **401**, 68–75 (2012).
30. Hu, Q. et al. Improved antifouling performance of a polyamide composite reverse osmosis membrane by surface grafting of dialdehyde carboxymethyl cellulose (DACMC). *J. Membr. Sci.* **620**, 118843 (2021).
31. Liu, Z. et al. Modification of thin film composite polyamide membranes with 3D hyperbranched polyglycerol for simultaneous improvement in their filtration performance and antifouling properties. *J. Mater. Chem. A* **5**, 23190–23197 (2017).
32. Hao, S. et al. Impact of hPG molecular size on the separation properties and antifouling performance of hPG-modified thin-film composite nanofiltration membrane. *Desalination* **548**, 116296 (2023).

33. Xu, J. et al. Positively charged aromatic polyamide reverse osmosis membrane with high anti-fouling property prepared by polyethylenimine grafting. *Desalination* **365**, 398–406 (2015).
34. Guan, Y. et al. Preparation of antifouling TFC RO membranes by facile grafting zwitterionic polymer PEI-CA. *Desalination* **539**, 115972 (2022).
35. Liu, M. et al. In situ modification of polyamide reverse osmosis membrane module for improved fouling resistance. *Chem. Eng. Res. Des.* **141**, 402–412 (2019).
36. Zhang, X. et al. Facile dual-functionalization of polyamide reverse osmosis membrane by a natural polypeptide to improve the antifouling and chlorine-resistant properties. *J. Membr. Sci.* **604**, 118044 (2020).
37. Li, S.-L. et al. Construction of pseudo-zwitterionic polyamide RO membranes surface by grafting positively charged small molecules. *Desalination* **537**, 115892 (2022).
38. Guo, J. et al. Membrane surface functionalization with imidazole derivatives to benefit dye removal and fouling resistance in forward osmosis. *ACS Appl. Mater. Interfaces.* **13**, 6710–6719 (2021).
39. Peng, L. E. et al. Does interfacial vaporization of organic solvent affect the structure and separation properties of polyamide RO membranes? *J. Membr. Sci.* **625**, 119173 (2021).
40. Liu, C., Faria, A. F., Ma, J. & Elimelech, M. Mitigation of biofilm development on thin-film composite membranes functionalized with zwitterionic polymers and silver nanoparticles. *Environ. Sci. Technol.* **51**, 182–191 (2017).
41. Peng, H. & Zhao, Q. A nano-heterogeneous membrane for efficient separation of lithium from high magnesium/lithium ratio brine. *Adv. Funct. Mater* **31**, 2009430 (2021).
42. Tiraferri, A. & Elimelech, M. Direct quantification of negatively charged functional groups on membrane surfaces. *J. Membr. Sci.* **389**, 499–508 (2012).
43. Yan, F. et al. Improving the water permeability and antifouling property of thin-film composite polyamide nanofiltration membrane by modifying the active layer with triethanolamine. *J. Membr. Sci.* **513**, 108–116 (2016).
44. Werber, J. R. et al. Materials for next-generation desalination and water purification membranes. *Nat. Rev. Mater.* **1**, 1–15 (2016).
45. Song, X. et al. Intrinsic nanoscale structure of thin film composite polyamide membranes: connectivity, defects, and structure–property correlation. *Environ. Sci. Technol.* **54**, 3559–3569 (2020).
46. Yahyaei, S., Vessally, E., Massoumi, B. & Rafati, M. DFT study of the interaction energy between thioglycoluril clip and phenol derivatives. *Phosphorus. Sulfur. Silicon. Relat. Elem.* **189**, 1417–1422 (2014).

Acknowledgements

We gratefully acknowledge the support of the China Postdoctoral Science Foundation (2021M702451), the National Natural Science Foundation of China (Nos. 21978215 and 22378314), Cangzhou Institute of Tiangong University (TGCYY-F-0101), Shandong Program of High-level Talents, and the Taishan Industrial Experts Program.

Author contributions

J.X.: Methodology, Writing-Original draft preparation, Data collection, Validation. S.H.: Conceptualization, Methodology, Visualization, Results Discussion, Writing- Reviewing and Editing, Funding Acquisition. Y.Q.: Methodology, Conceptualization. P.Q.: Methodology. Z.Z.: Methodology, Conceptualization. Y.H.: Supervision, Conceptualization, Data Analysis, Results Discussion, Funding Acquisition, Writing-Reviewing and Editing. J.X. and S.H.: are considered “co-first author”.

Competing interests

The authors declare no competing interests.

Additional information

Supplementary information The online version contains supplementary material available at https://doi.org/10.1038/s41545-024-00326-5.

Correspondence and requests for materials should be addressed to Yunxia Hu.